ACS OMEGA

http://pubs.acs.org/journal/acsodf

Article

Drug Delivery from PCL/Chitosan Multilayer Coatings for Metallic Implants

Íris Soares, Jaime Faria, Ana Marques, Isabel A. C. Ribeiro, Carlos Baleizão, Ana Bettencourt, Isabel M. M. Ferreira, and Ana Catarina Baptista*

Cite This: *ACS Omega* 2022, 7, 23096−23106

Read Online

ACCESS | Metrics & More | Article Recommendations | Supporting Information

ABSTRACT: Implant-related infections, mainly caused by *Staphylococcus aureus*, are a major health concern. Treatment is challenging due to multi-resistant strains and the ability of *S. aureus* to adhere and form biofilms on bone and implant surfaces. The present work involved the preparation and evaluation of a novel dual polymeric film coating on stainless steel. Chitosan and polycaprolactone (PCL) multilayers, loaded with poly(methyl methacrylate) (PMMA) microspheres encapsulating vancomycin or daptomycin, produced by the dip-coating technique, allowed local antibiotic-controlled delivery for the treatment of implant-related infections. Enhanced adhesion of the film to the metal substrate surface was achieved by mechanical abrasion of its surface. Studies have shown that for both drugs the release occurs by diffusion, but the release profile depends on the type of drug (daptomycin or vancomycin), the pH of the solution, and whether the drug is freestanding (directly incorporated into the films) or encapsulated in PMMA microspheres. Daptomycin freestanding films reached 90% release after 1 day at pH 7.4 and 4 days at pH 5.5. In comparison, films with daptomycin encapsulated microspheres reached 90% release after 2 h at pH 5.5 and 2 days at pH 7.4. Vancomycin encapsulated and freestanding films showed a similar behavior reaching 90% release after 20 h of release at pH 5.5 and 2 and 3 days, respectively, at pH 7.4. Furthermore, daptomycin-loaded films showed activity (assessed by agar diffusion assays) against sensitive (ATCC 25923) and clinically isolated (MRSA) *S. aureus* strains.

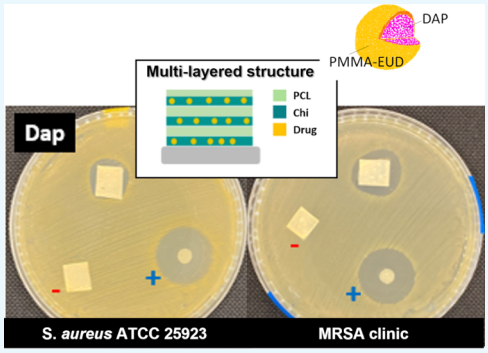

1. INTRODUCTION

Bone infection related to the use of orthopedic implants is associated with complications following surgery and device implantation, leading to implant failure, and resulting in diseases such as osteomyelitis and septic arthritis that lead to necrosis and bone destruction.[1] Nowadays, with sterility within the operating room and protocols of perioperative antibiotic prophylaxis, there is a decrease in the incidence of infections associated with orthopedic implants. Nevertheless, implant infection risk is still estimated to be 0.5−5%, representing the number one cause of implant failure,[2] with reinfection occurring in 10−30% of cases.[3] When an infection is diagnosed, several therapeutic approaches may be adopted. Preoperative procedures involve antibiotic prophylaxis[4,5] or sonication of the implant to remove any adhered biofilm.[6] Postoperative procedures include systemic antibiotics for a prolonged period of time and wound debridement and lavage.[4] These treatments, however, are not always effective on already established infections. Often, prosthesis removal and replacement, or even joint fusion, are the only solutions to definitively eradicate severe infections.[2] Furthermore, antibiotic therapy is long-lasting, and to achieve effective therapeutic drug concentration at the site of infection, a high parenteral dose of antibiotic is needed, which can lead to systemic toxicity.[7]

New approaches have been sought after, in the form of antimicrobial surfaces, that can be divided into structured surfaces, permanent antimicrobial surfaces, and elution systems.[8,9] Structures such as nanoparticle- and nanotube-modified surfaces,[10,11] and engineered metal topographies such as alterations in charge, hydrophobicity, roughness, and porosity[9,12,13] have been studied. Permanent antimicrobial surfaces, that contain permanently bonded agents that generate antimicrobial surfaces and prevent long-term bacterial adhesion[14,15] have also been created.[16−18] To further improve the antimicrobial effect of implants, studies veered into the usage of drugs in their composition, via the creation of elution systems, that actively release antimicrobials to inhibit bacterial adhesion and/or promote bacterial cell death in both the implant and adjacent tissues.[9] For instance, Kazemzadeh-Narbat et al. developed a layer-by-layer thin film for prolonged antimicrobial peptide (AMP) release on Ti implants enabling

Received: January 25, 2022
Accepted: May 13, 2022
Published: June 28, 2022

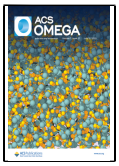

controlled and sustained release of an AMP showing antibacterial activity against *Staphylococcus aureus*.[19] Nablo et al. coated medical-grade stainless steel with a sol−gel film of 40% *N*-aminohexyl-*N*-aminopropyltrimethoxysilane and 60% isobutyltrimethoxysilane for the release of nitric oxide (NO) against *S. aureus* that enabled a diminished bacterial adhesion.[20]

These active attack surfaces, however, still have issues such as the accumulation of dead bacteria and debris, that shield the surface, reducing the bactericidal effect and providing nutrients for subsequent bacterial adhesion. To avoid these issues, studies have focused on surfaces with different parts, called units, one responsible for killing bacteria and one responsible for releasing the dead bacteria from the surface. To do such, responsive systems are often incorporated into the coatings. In principle, these will realize both passive and active functions simultaneously to improve the overall antibacterial efficacy.[21]

In this work a 316L stainless steel (SS) coated with multilayered chitosan (Chi) and polycaprolactone (PCL) is proposed as a novel sustained drug release system, these polymers are chosen for their known biocompatibility and ease of processing. Several functional coatings have been reported to improve the biocompatibility, and antimicrobial and drug release performances of metallic implants.[22] Some examples are calcium phosphates,[23] titanium oxides,[24] and polymer composites with antibacterial properties.[25] In this study, 316L-SS has been selected as the substrate for this study since it is low-cost and often used for metal implant fabrication.[26] The Chi layers should contain one of two antibiotics, daptomycin (Dap) or vancomycin (Van) encapsulated on acrylic-based (PMMA or PMMA-EUDRAGIT RL-100) microspheres via a previously reported method.[27] A PCL film was deposited on the top of the Chi layer to slow down and control the drug release. Dap has been suggested as an effective alternative to Van, which has been one of the antibiotics of choice for bone infection treatment but has shown increasing bacterial resistance.[28] The proposed coating relies on the incorporation of PMMA microspheres for a controlled drug release following an optimal release pattern of a burst release followed by sustained release, and in the inherent polymer properties enabling a pH response, and thus a smart release system that allows drug release at pH values representative of an infection environment. Apart from this, the construction of both passive and active functions via the layer-by-layer system also discards the problem often observed in these dual systems since bactericidal components usually bind to bacteria and the non-fouling components repel bacteria.[21]

2. EXPERIMENTAL SECTION

2.1. Surface Treatment of Substrates. Commercially available 0.1 mm thick 316L-SS substrates (AISI 316L, Fe/Cr_{18}/Ni_{10}/Mo_3 Goodfellow, England) were cleaned for 5 min in sequential ultrasound baths of ultrapure water and acetone (96%, Labchem, Portugal), and then placed in an oven at 300 °C for 10 min, followed by 10 min in sequential ultrasound baths of ultrapure water and acetone (96%, Labchem, Portugal). Next, these were treated with silica sandpaper (1000 grit, Dexter) by hand. The surface was scribed 100 times in vertical, horizontal, and circular directions as shown in the schematics of Figure S1A. After the treatment, the substrates were again cleaned for 15 min in sequential ultrasound baths of ultrapure water, ethanol (96% v/v), and toluene. Removal of toluene was done by SS drying in a vacuum chamber at 70 °C and a pressure of 1 bar for 90 min.

2.2. Production of PMMA Microspheres. PMMA (350 kDa, Sigma-Aldrich) and PMMA-EUDRAGIT (Evonik Degussa International AG, Spain) (PMMA-EUD) microspheres, loaded with Van and Dap respectively, as well as unloaded, were produced using a previously reported methodology.[27] Briefly, PMMA or polymer blends of PMMA-EUD (30 w/w) were dissolved in 5 mL of dichloromethane (Fisher Scientific) and emulsified by homogenization using an Ultra-Turrax T10 basic (IKA, Staufen, Germany) for 3 min with a 10% (w/w) poly(vinyl alcohol) (PVA) solution (13−23 kDa, 87−89% hydrolyzed, Sigma-Aldrich), where the antibiotics, daptomycin (Cubicin, 350 mg, Novartis Pharma AG, Switzerland) or vancomycin (Vancomicina Generis 1000 mg, Generis Farmacêutica, S.A., Portugal) were previously solubilized (15% w/w). The resulting water−oil (w1/o) emulsion was added to 30 mL of 1.25% (w/w) PVA solution and emulsified by homogenization using a Silverson Laboratory Mixer Emulsifier L5 M (Silverson Machines Inc., Chesham, U.K.) for 10 min at 20 L/min (maximum mixing speed). The resulting w1/o/w2 double emulsion was magnetically stirred at room temperature for 4 h to evaporate the organic solvent. PMMA and PMMA-EUD particles were harvested by centrifugation (Beckman Coulter Inc., Fullerton), washed three times with 5723*g*, 10 min, 4 °C; Allegra 64R high speed centrifuge, a 10% (w/v) sucrose solution, and resuspended in a 0.5% (w/v) sucrose solution. All particles were subsequently freeze-dried (Christ α 1−4, B. Braun Biotech International, Melsungen, Germany) to obtain a fine, free-flowing dry powder. All batches were prepared in triplicate and plain (without drugs) particles were used as controls. For characterization, encapsulation efficiency (EE), drug loading (DL), and particle size were analyzed by ultraviolet−visible (UV−vis) spectroscopy and scanning electron microscopy (SEM).

Average particle diameter was calculated from SEM micrographs using ImageJ software, measuring 30 randomly selected spheres from each sample. EE and DL were calculated using the supernatant obtained during the washing step of microsphere production, cumulative of the sequential centrifugations of the microsphere solutions. The amount of drug contained in the supernatant was estimated from UV−visible absorbance spectra obtained for a 200 μL sample. The drugs were quantified by UV−visible spectrophotometry (FLUOstar Omega, BMG Labtech), at 365 nm for daptomycin and 230 nm for vancomycin. Encapsulation efficiency refers to the percentage of the encapsulated drug compared to the initial amount used for particle preparation (eq 1), the encapsulated drug is considered as the initial drug added minus the drug present in the supernatant.

$$\mathrm{EE}(\%) = \frac{\text{encapsulated drug}}{\text{initial drug}} \times 100 \quad (1)$$

Drug loading refers to the weight percentage ratio of the drug in the microspheres (eq 2), the drug content in the microspheres is calculated using the amount of drug added initially and the EE.

$$\text{drug loading}(\%) = \frac{\mathrm{EE} \times \text{initial drug mass}}{\text{particle mass}} \times 100 \quad (2)$$

2.3. Preparation of Polymer-Based Solutions and Films. Chitosan (low molecular weight, Sigma-Aldrich,

https://doi.org/10.1021/acsomega.2c00504
ACS Omega 2022, 7, 23096−23106

Iceland) was dissolved in a solution of 1:1 v/v of ethanol (Honeywell, Germany, ≥99.8%) and 1% acetic acid (HAc) (Sigma-Aldrich, Germany, ≥99.7%) in ultrapure water to obtain a polymer concentration of 0.04% w/v. The solution was kept under magnetic agitation for 12 h at room temperature and then kept in a sealed flask. PCL (Sigma-Aldrich, U.K., 80 kDa) was mixed with dichloromethane (Carlo Erba, France) at a concentration of 0.1% w/v and stirred under magnetic agitation at room temperature for 12 h, and then kept in a sealed flask. Chitosan solutions with Dap or Van or the produced acrylic microspheres containing them were obtained by the addition of these components to the polymeric solution at concentrations of 0.8 mg/mL (for freestanding drug) and 4 mg/mL (for encapsulated drug) and subsequent magnetic agitation of the solutions obtained. The solutions were kept in sealed flasks.

A dip-coating system with a stirrer (SILAR model HO-TH-03A) was used and the parameters for all dip-coating procedures were set: retrieval speed—10 mm/s, dip duration—5 s, drying time after dip—1 min, and arm rotation speed—5 mm/s; solutions were used at room temperature. Films of alternating chitosan and PCL layers were made, with freestanding or encapsulated drug, or no drug at all incorporated into the chitosan layer. A total number of 6 layers were deposited, with the chitosan layer directly in contact with the metal.

2.4. Characterization. Characterization of the surface morphology of the SS substrates, before and after the mechanical treatment, was performed with an atomic force microscope of WITec α 300 RAS confocal spectrometer. The cantilever was operated with a WITec Arrow Al coated probe in tapping mode at 75 kHz and a constant load of 2.8 N/m. The acquired topography map of 30 μm^2 shown in the Supplementary Information was used to extract the surface roughness (using WiTecProject software).

An average thickness of polymer-based films was obtained using a digital micrometer (Mitutoyo, Japan). Film adhesion was tested by the 180° peel-off method adapted from[29] and schematically presented in Figure 1.

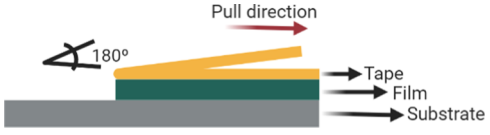

Figure 1. Schematic representation of 180° peel-off tests showing a substrate (gray) with the deposited film (dark green) covered by tape (orange) with the tape removal direction denoted by the arrow.

The films were covered with a strip of tape and the tape was pulled off at a constant force using a traction machine 20 N load cell Rheometric Scientific uniaxial machine operable using "Minimat" software (Minimat Control Software version 1.60 February 1994 (c) P.L. Thermal Science 1984−94 Rheometric Scientific Ltd.). For all peel-off tests, the tape used was Tesa basic packaging tape-58572 and was fixed to the moving claw.

The optical images of the samples were obtained using a Leica DMi8 inverted microscope and images were obtained in reflective mode. Samples of the microspheres and SS substrates were analyzed by SEM (Hitachi model 2400) after surface treatment, film deposition, and peel-off tests to evaluate sample morphology and film porosity. Before analysis, all samples were cut and placed on a SEM disk using carbon tape and then sputter-coated with a gold/palladium (Au−Pd) coating. The same coating was also applied to the microparticles after their suspension in ethanol (96% v/v), which were directly placed on the carbon tape.

Confocal Raman spectrophotometer (Witec α 300 RAS) using a laser with a wavelength of 532 nm and 30 mW of power for sample composition characterization and for tracking Dap and Van in the microspheres and the obtained films. Composition homogeneity was further studied through Raman mapping of drug microsphere-loaded films in small 5 μm^2 surface areas.

Pore size and density were accessed using ImageJ software and measuring the diameter of 10 pores. The pore density was made by calculating the total number of pores and dividing it by the area of the film.

2.5. In Vitro Drug Release Tests. Calibration curves for daptomycin and vancomycin in simulated body fluid (SBF) at 2 pH values (7.4, and 5.5) were obtained using UV−vis spectroscopy (T90+ UV−vis spectrometer from PGInstruments Ltd.) at 262 nm for Dap and 280 nm for Van. The SBF solution was made following the protocol described by Kokubo et al.[30] and then kept in a refrigerator until use. The pH 7.4, corresponds to the normal physiological pH and pH 5.5 to the pH that exists in a stage of infection. For calibration curves, concentrations of 666, 500, 333, 250, 167, 125, 83.2, 62.5, 31.2, 15.6, 7.81 and 3.9 μg/mL were studied.

Drug release studies were conducted by placing the films inside a 4 mL screw cap plastic vials and submerging them in 500 μL of SBF with a pH of 5.5 and 7.4 at 37 °C. At predetermined time intervals, the SBF was removed from the vial, and replaced by an equal amount of new SBF. The SBF was analyzed by UV−vis spectroscopy using a Rotilabo quartz cuvette with a path length of 1 cm and a maximum volume of 0.7 μL. This analysis was made for five replicas of each film for a total period of 120 h.

2.6. Antibacterial Assay. The direct testing of the antimicrobial activity of the samples against *S. aureus* ATCC 25923 and MRSA (clinical isolated) was determined by agar diffusion as previously described.[31] Shortly, for the agar diffusion assay, isolated colonies were suspended in Mueller Hinton Broth (MHB, Biokar Diagnostics, France) and diluted until achieving ≅ 1×10^8 CFU/mL. The inoculum was swabbed uniformly on Muller Hinton Agar (MHA, Biokar Diagnostics, France) plates. The tested samples and filter-paper disks (6 mm diameter) with 10 μL of daptomycin or vancomycin at 3 mg/mL (positive control) were placed on the agar surface. Next, the plates were incubated at 37 °C for 24 h and the inhibition zone diameters were measured with a digital Vernier caliper. Samples of the Chi/PCL film with both encapsulated drugs were tested, and the films with empty microspheres were used as a negative control.

3. RESULTS AND DISCUSSION

3.1. PMMA Microspheres. Particle diameter, EE, and DL of the particles produced were determined. Regarding particle diameter, SEM images of PMMA, PMMA-Van, PMMA-EUD, and PMMA-EUD-Dap particles (Figure 2) show spherical particles with a relatively low size dispersion and a higher aggregation for PMMA-EUD microspheres. As expected, the diameters obtained show that the spheres were in the micro-size range (1.29 ± 0.13 μm for PMMA; 1.15 ± 0.28 μm for PMMA-Van; 0.96 ± 0.25 μm for PMMA-EUD, and 0.68 ± 0.11 μm for PMMA-EUD-dap).

https://doi.org/10.1021/acsomega.2c00504
ACS Omega 2022, 7, 23096−23106

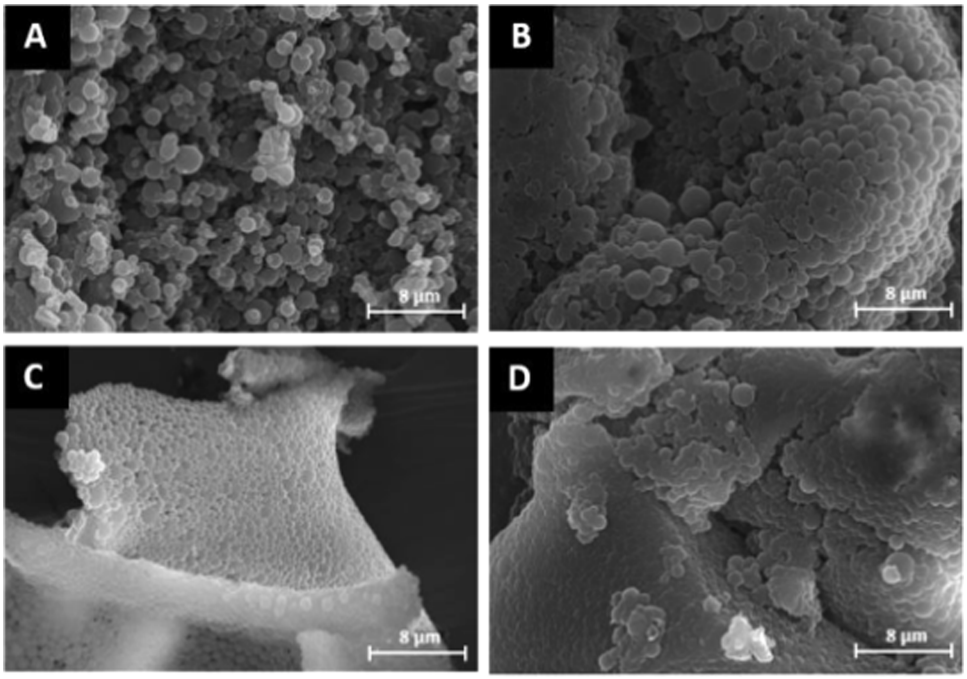

Figure 2. SEM micrographs of the obtained microspheres showing: (A) PMMA, (B) PMMA-Van, (C) PMMA-EUD, and (D) PMMA-EUD-Dap microspheres.

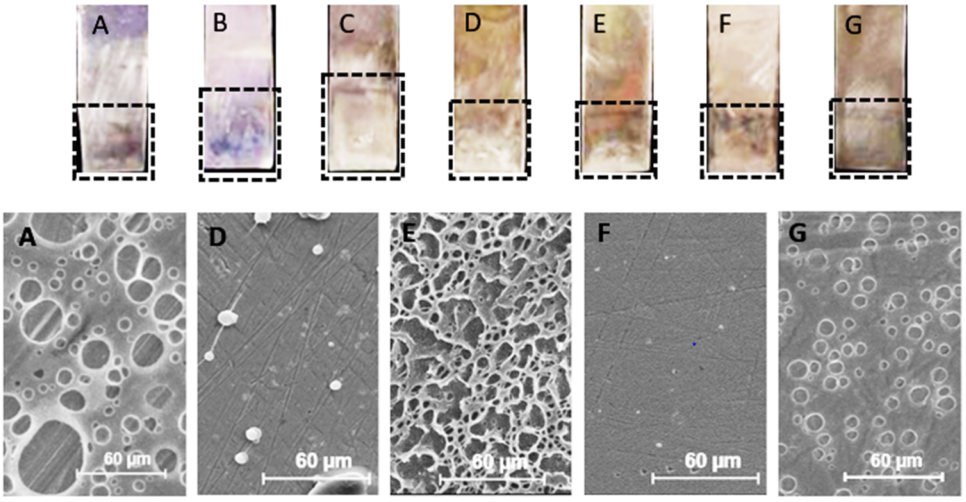

Figure 3. Chitosan/PCL films with (A) no drugs or microspheres (Chi/PCL), (B) PMMA microspheres (Chi/PCL-PMMA), (C) PMMA-EUD microspheres (Chi/PCL-PMMA-EUD), (D) PMMA-Van microspheres (Chi/PCL-PMMA-Van), (E) PMMA-EUD-Dap microspheres (Chi/PCL-PMMA-EUD-Dap), (F) vancomycin (Chi/PCL-Van), and (G) daptomycin (Chi/PCL-Dap) and respective SEM images.

EE values of daptomycin and vancomycin were 97.20 ± 1.20% and 97.89 ± 0.04%, respectively. These values are in accordance with the literature[27] that refers to an EE value of 91.1 ± 0.7% for Van and 95.6 ± 1.2% for Dap. DL values obtained were 21.64 ± 0.67% for Dap and 22.55 ± 2.73% for Van which is almost double the values reported for this process, 12.4 ± 0.3 and 11.9 ± 0.1% respectively.[27]

3.2. PCL and Chi Coatings on Stainless Steel Substrates. After microsphere production, polymeric films were produced, for later microsphere incorporation. For this purpose, chitosan and PCL coatings were deposited on stainless steel, with polymeric solutions being altered to increase the adhesion and improve film uniformity. After preliminary tests, a chitosan concentration of 0.04% w/v and a PCL concentration of 0.1% w/v proved to be the best for film adhesion and uniformity. These films kept their properties even after the addition of the drugs at a concentration of 0.8 mg/mL or microspheres at a concentration of 4 mg/mL, the concentrations were made such that the amount of drug was the same in freestanding and encapsulated forms. SEM images of the deposited films (Figure 3) show that the surface of both Chi/PCL-PMMA-Van and Chi/PCL-Van films are smooth with visible lines of the surface treatment.

The presence of microspheres on the Chi/PCL-PMMA-Van film surface is observed, indicating sphere transference from the film to the PCL solution during the dip-coating process.

Both PCL/Chi-PMMA-EUD-Dap and Chi/PCL-Dap films have a porous surface with average pore sizes of 1.38 ± 3.00 and 0.94 ± 0.25 μm, respectively, and pore densities of 0.476 ± 0.041 and 0.136 ± 0.012 pore/μm^2, respectively. In the

https://doi.org/10.1021/acsomega.2c00504
ACS Omega 2022, 7, 23096−23106

microsphere-loaded films, the lines from the metal treatment are not observed, indicating a thicker film than the Chi/PCL-Dap film where these lines are visible. The unloaded PCL/Chi films also show a porous surface with an average diameter of 2.56 ± 1.85 μm and a pore density of 0.180 ± 0.027 pore/μm^2.

Table 1 presents the average thickness for each type of film along with the adhesion obtained from the pill-off tests. In general, results show a good thickness uniformity for all samples except for the Chi/PCL-Dap and Chi/PCL-PMMA films, in which accumulation of polymeric solution in one area upon drying may have occurred. The peel-off of all samples showed a cohesive failure, meaning that the detachment occurred between the film layers, and not due to adhesive failure i.e., detachment between the sample and the metal. This reveals that the adhesion forces between film and metal are stronger than those between film layers. The average peel-off forces (Table 1) are in the range of 0.57−0.95 N, indicating the variation associated with the process used, since manual adhesion of the tape to the samples leads to variations in adhesion between the two. Overall, it can be concluded that film adhesion is not affected by their composition. The peel-off curves obtained are similar to those found in the literature[29] with areas of the curve showing the peeling of the film and tape or just the peeling of the film alone (Figure S2).

Table 1. Average Film Thickness (n = 30) and Peel-Off Forces Obtained by the Peel-Off Test (n = 15)

film	thickness (μm)	adhesion (N)
Chi/PCL	6.5 ± 1.5	0.57 ± 0.13
Chi/PCL-Dap	20 ± 9.5	0.92 ± 0.17
Chi/PCL-Van	40 ± 2.0	0.68 ± 0.22
Chi/PCL-PMMA-EUD	9.0 ± 1.0	0.73 ± 0.36
Chi/PCL-PMMA-EUD-Dap	4.0 ± 1.0	0.63 ± 0.22
Chi/PCL-PMMA	4.0 ± 2.5	0.72 ± 0.21
Chi/PCL-PMMA-Van	8.0 ± 2.0	0.60 ± 0.19

3.4. Drug Content in Films and Microcapsules. Raman spectra of raw materials used in the fabrication of the polymeric films (chitosan and PCL) and microspheres (PMMA or PMMA-EUD) with and without the drug (Van or Dap) inside are shown in Figure 4A. In this set of spectra, the spectral signature of each material is perceived but more importantly, spectral comparison allowed the identification of characteristic peaks from the two drugs (e.g., V_1, V_2, and D_2), i.e. of molecular vibration modes not existing in the spectra of other materials. For vancomycin, prominent vibration modes are ν(CC) skeletal mode bond, ν(C−N) of amide-III, δ(C−H) of CH_2 and CH_3, ν(C═O) of amide-I, and ν(C═C), which can be found at 990, 1242, 1334, 1602 cm^{-1} (V_1), and 1678 cm^{-1} (V_2), respectively.[32] For daptomycin, Raman peak identification is lacking in the literature, however, D2 is associated with the $CONH_2$ group, referred to as the amide-II (1549 cm^{-1}) and amide-I (1638 cm^{-1}) bands, compatible with the molecular configuration and the spectroscopic literature of amide bands.[33] Chemically, Dap comprises 13 amino acids, including several non-standard and D-amino acids, with the C-terminal 10 amino acids forming an ester-linked ring and the N-terminal tryptophan covalently bonded to decanoic acid.

Tracking the selected characteristic peaks in the Raman spectra of drug microspheres in Figure 4B and of films made with drugs added to the chitosan layer in the form of microspheres or freestanding powder in Figure 4C,D, respectively, provides significant information about sample composition. All Raman spectra are shown in the region of 200−2000 cm^{-1} since it comprises most of the material's molecular vibration modes and only excludes the typical fluorescence shoulder (still visible in the spectrum left edge) and the modes: CH_2 and CH_3 (stretching), olefinic C−H (symmetric and asymmetric), and OH (stretching). The bands of this latter mode are in the wavenumber ranging from 3200 to 3400 cm^{-1} and are only characteristic of Van, Dap, and Chi molecules. Nevertheless, these OH-stretching modes were only detected in the spectra of raw materials. These show typical molecular vibration modes of organic compounds, mainly associated with carbon−oxygen, carbon−carbon, carbon−hydrogen groups, and amide groups for the drugs and chitosan. Peak identification was made according to the literature for all the used materials except for Dap. Nevertheless, since the characteristic peaks marked in Figure 4A (V1, D1, and D2) for Van and Dap are clearly identified in the Raman spectra of drug-containing microspheres in Figure 4B, and absent in the empty polymeric microspheres, then Van is included in the PMMA microspheres and Dap in the PMMA-EUDRAGIT microspheres, either on their surface or inside them. Nevertheless, as shown in Figure 4C, when these microspheres are added to the Chi layer of PCL/Chi films, only Van is detected. Furthermore, none of the drugs added to the Chi layer of the PCL/Chi films in the powder form could be detected. This may be due to the low concentrations (trace level) of drugs added to the films, which have a stronger signal, masking the drug signal which also agrees with the small signal detected for microspheres containing the drug. Another possible cause is the un-homogeneous drug distribution along the film. In this case, the drugs may be difficult to detect using a standard single spectrum Raman spectroscopy strategy. Therefore, for further investigating drugs spread over the chitosan film area, Raman mapping was also performed.

Figure 5 shows the 5 × 5 μm^2 Raman maps acquired for the PCL/Chi films loaded with the polymeric drug microspheres of Dap (A) and Van (B), and for PCL/Chi films loaded with Van powder (C). Comparing Figure 5B,C it is possible to verify that the Van seems to be more homogeneously distributed (either when enclosed in the PMMA microspheres or added as powder) than Dap enclosed in PMMA-EUD microspheres. Nevertheless, that correlates with the PCL distribution, since the drug signal is undetectable when the PCL signal is stronger, perhaps indicating that PCL is not a completely continuous film regarding its thickness. This evidence may explain why vancomycin was detected in the single point Raman spectra shown in Figure 4C but not daptomycin. Also, Van seems to be more homogeneously distributed when loaded as powder directly in the films than when inside the microsphere. Because as powder, Van concentration is low across the film, and it is more difficult to detect this drug when added in the form of powder. Furthermore, since in the freestanding drug film PCL distribution is also more uniform, one may think that the microspheres may create thicknesses discontinuities, facilitating drug visualization in the films with microspheres.

In Figure 5A is still interesting to note that, as expected PMMA and Dap have the same distribution over the surface evidencing that Dap maybe inside PMMA and that, their distribution is only detected when the detected signal from the PCL is in fact not detected or it is stronger, which suggests that PCL is on top of the chitosan layer where the drug

https://doi.org/10.1021/acsomega.2c00504
ACS Omega 2022, 7, 23096−23106

Figure 4. Raman spectra of (A) film compounds, (B) PMMA and PMMA-EUDRAGIT microspheres with and without vancomycin and daptomycin inside, respectively, (C) PCL/chitosan films with drug-loaded microspheres added to the chitosan layer, and (D) PCL/chitosan films with drugs added to the chitosan layer as freestanding powders.

microspheres are. This is corroborated by the similar chitosan, PMMA, and Dap areal distributions.

3.5. Drug Release. In vitro release assays indicate that the pH of the surrounding media affects the drug release profiles for all the tested drug-loaded films (Figure 6). The total time of release was 120 h.

Further, the data of the in vitro release tests were fitted to various kinetic models, namely, the zero-order, first-order, Hixon−Crowell, Higuchi, and Korsmeyer−Peppas models[34] (Table 2).

Drug release was plotted according to each model and the corresponding fits were made. R^2 values were then obtained, and it was considered that the kinetic model for the drug release was the one in which the fitting had a higher R^2 value. When the model obtained was the Korsmeyer−Peppas, the value of the constant n, that is the exponent of release, and related to the drug release mechanism, was also obtained. Depending on the value of n, the mechanisms were identified as quasi-Fickian if $n < 0.5$, Fickian if $n = 0.5$, and non-Fickian or anomalous transport if $0.5 < n \leq 1$.[34]

With respect to the mechanism of kinetics (Table 2) the results show that Dap films follow a Korsmeyer−Peppas model, with n values of 0.13 and 0.21 and R^2 values of 0.94 and 0.92 for pH values of 7.4 and 5.5, respectively, indicating quasi-Fickian release mechanisms for all pH values. This indicates that for the films with the microspheres, drug release is affected by both diffusion and polymer swelling[34]

Films with freestanding Dap show a first-order release value of 7.4, with an R^2 value of 0.77, and Korsmeyer−Peppas model for a pH value of 5.5 with an R^2 value of 0.92 with an n value of 0.16 indicating a quasi-Fickian mechanism.[34]

Films with encapsulated Van show a 1st order release mechanism for pH values of 7.4 and 5.5 with R^2 values of 0.98 and 0.90, respectively. Films with freestanding Van follow a

https://doi.org/10.1021/acsomega.2c00504
ACS Omega 2022, 7, 23096−23106

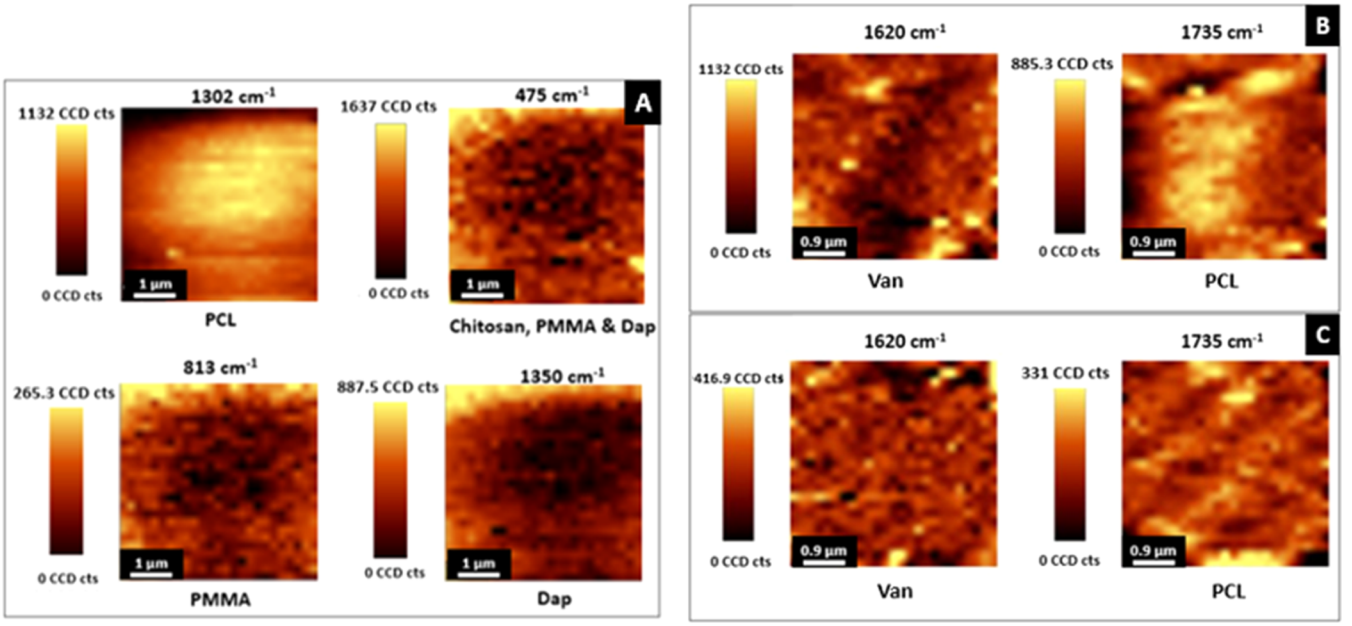

Figure 5. Raman maps acquired in an area of 5 × 5 μm^2 of PCL/Chi films loaded with Dap (A) and Van microspheres, as well as in PCL/Chi films loaded with Van added to the Chi layer in the powder form. Each pixel in the map corresponds to the integral of materials' characteristic peaks cantered at the marked positions in wavenumbers. In Figure 5A the considered characteristic peaks were: 475 cm^{-1} for the film (in chitosan, PMMA, and Dap spectra) 813 cm^{-1} for PMMA, 1302 cm^{-1} for PCL, and 1350 cm^{-1} for Dap; and in (B) and (C) a broader integral band was considered for the Van maps, (centered at 1620 cm^{-1} with a width of 160 cm^{-1}, covering V1 and V2 peaks) and for the film, the PCL peak at 1735 cm^{-1} was considered.

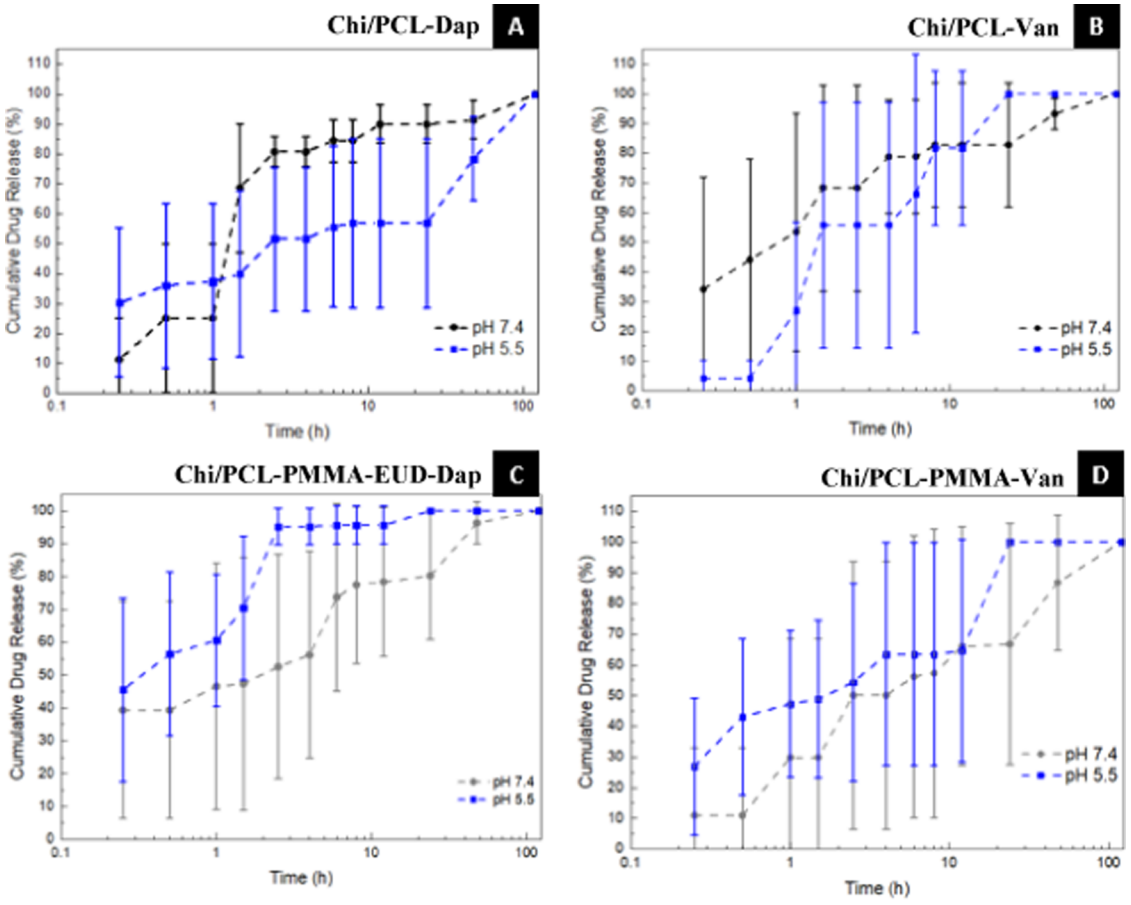

Figure 6. Cumulative drug release plot from (A) Chi/PCL-Dap, (B) Chi/PCL-Van, (C) Chi/PCL-PMMA-EUD-Dap, and (D) Chi/PCL-PMMA-Van films plotting the percentage of drug released versus time (n = 5) for pH values of 5.5 and 7.4. The total time of release was 120 h.

https://doi.org/10.1021/acsomega.2c00504
ACS Omega 2022, 7, 23096−23106

Table 2. Fitted Parameter Values and R^2 for the Different Equation Models Used to Determine the Release Mechanism of the Drugs from the Films[a]

release model	Sample	pH = 7.4	pH = 5.5
zero-order (Mt = k_0t)	Chi/PCL-PMMA-EUD-Dap	k_0 (h^{-1}) = 0.31	k_0 (h^{-1}) = 0.16
		R^2 = 0.42	R^2 = 0.15
	Chi/PCL- Dap	k_0 (h^{-1}) = 0.29	k_0 (h^{-1}) = 0.35
		R^2 = 0.20	R^2 = 0.76
	Chi/PCL-PMMA-Van	k_0 (h^{-1}) = 0.42	k_0 (h^{-1}) = 0.33
		R^2 = 0.52	R^2 = 0.39
	Chi/PCL-Van	k_0 (h^{-1}) = 0.28	k_0 (h^{-1}) = 0.39
		R^2 = 0.32	R^2 = 0.29
first-order (Mt = $1-e^{-k1t}$)	Chi/PCL-PMMA-EUD-Dap	k_1 (h^{-1}) = 25.1	k_1 (h^{-1}) = 21.1
		R^2 = 0.77	R^2 = 0.73
	Chi/PCL- Dap	k_1 (h^{-1}) = 32.6	k_1 (h^{-1}) = 22.4
		R^2 = 0.77	R^2 = 0.91
	Chi/PCL-PMMA-Van	k_1 (h^{-1}) = 33.1	k_1 (h^{-1}) = 27.6
		R^2 = 0.98	R^2 = 0.90
	Chi/PCL-Van	k_1 (h^{-1}) = 18.3	k_1 (h^{-1}) = 39.7
		R^2 = 0.49	R^2 = 0.89
Hixson–Crowell ($\sqrt[3]{M}t = k_{HC}t$)	Chi/PCL-PMMA-EUD-Dap	k = 0.49	k = 0.49
		R^2 = 0.48	R^2 = 0.15
	Chi/PCL- Dap	k_{HC} = 1.07	k_{HC} = 1.1
		R^2 = 0.12	R^2 = 0.74
	Chi/PCL-PMMA-Van	k_{HC} = 1.00	k_{HC} = 1.0
		R^2 = 0.48	R^2 = 0.39
	Chi/PCL-Van	k_{HC} = 1.16	k_{HC} = 1.2
		R^2 = 0.32	R^2 = 0.21
Higuchi (Mt = $k_H\sqrt{t}$)	Chi/PCL-PMMA-EUD-Dap	k_H($h^{-1/2}$) = 0.15	k($h^{-1/2}$) = 0.082
		R^2 = 0.42	R^2 = 0.38
	Chi/PCL- Dap	k_H($h^{-1/2}$) = 0.14	k_H($h^{-1/2}$) = 0.18
		R^2 = 0.2	R^2 = 0.74
	Chi/PCL-PMMA-Van	k_H($h^{-1/2}$) = 0.21	k_H($h^{-1/2}$) = 0.17
		R^2 = 0.5	R^2 = 0.44
	Chi/PCL-Van	k_H($h^{-1/2}$) = 0.14	k_H($h^{-1/2}$) = 0.19
		R^2 = 0.32	R^2 = 0.28
Korsemeyer–Peppas (Mt = $k_{KP}t^n$)	Chi/PCL-PMMA-EUD-Dap	k_{KP}($h^{-1/2}$) = 5.29	k_{KP}($h^{-1/2}$) = 5.98
		R^2 = 0.93	R^2 = 0.92
		n = 0.13	n = 0.21
	Chi/PCL- Dap	k_{KP}($h^{-1/2}$) = 4.31	k_{KP}($h^{-1/2}$) = 4.90
		R^2 = 0.94	R^2 = 0.92
		n = 0.13	n = 0.21
	Chi/PCL-PMMA-Van	k_{KP}($h^{-1/2}$) = 3.86	k_{KP}($h^{-1/2}$) = 5.15
		R^2 = 0.91	R^2 = 0.73
		n = 0.54	n = 0.24
	Chi/PCL-Van	k_{KP}($h^{-1/2}$) = 5.58	k_{KP}($h^{-1/2}$) = 3.45
		R^2 = 0.99	R^2 = 0.79
		n = 0.32	n = 1.07

[a]Mt denotes the fraction of drug released up to time t; k_0, k_1, k_{HC}, k_H, and k_{KP} are constants of the mathematical models; n is the release exponent of the Korsmeyer–Peppas model.

Korsmeyer–Peppas model for a pH of 7.4, with an R^2 of 0.99 and an n value of 0.32, again, indicating a quasi-Fickian mechanism, and the first-order kinetics for pH value of 5.5 with an R^2 of 0.89.[34]

3.6. Antibacterial Assay. The disk diffusion test was used for screening the antibacterial activity of the drug-loaded films. This test provides an opportunity for the quick estimation and a comparison of antibacterial activity of novel delivery platforms with the free drug.[35] The results showed that the Dap-loaded films effectively inhibited bacterial growth, with the inhibition zone diameters of ∼14 and ∼17 mm for sensitive and resistant strains, respectively (Figure 7). No inhibition zone could be observed for the sample without antibiotics (negative control). Van-loaded films also show no antibacterial activity, which may be due to a low diffusion of the drug in the agar medium or diffusion that lies below the vancomycin MIC reported for *S. aureus*, 2 μg/mL for the ATCC 25923 strain,[12] and from 4 to 8 μg/mL for VRSA.[36] Moreover, results of positive antibiotic control were in accordance with the expectable inhibition halos described in the literature as 18–23[37] and 17–21[38] for Dap and Van respectively, toward *S. aureus* ATCC 25923 assuring the assay suitability.

https://doi.org/10.1021/acsomega.2c00504
ACS Omega 2022, 7, 23096−23106

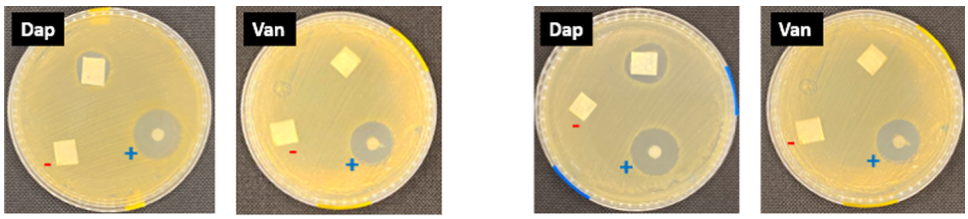

	Daptomycin		Vancomycin	
Strain	Sample	Control	Sample	Control
S. aureus ATCC 25923	13.9 ± 1.3 mm	20.6 ± 0.2 mm	-	20.1 ± 0.9 mm
MRSA clinic	16.6 ± 2.2 mm	21.7 ± 0.4 mm	-	21.7 ± 1.0 mm

Figure 7. Antibacterial assay for encapsulated drug films showing positive (plus sign) and negative (minus sign) control and sample's diameter of inhibition zones (in mm) obtained for encapsulated drug films against two strains of *S. aureus*.

4. CONCLUSIONS

Multilayer films of chitosan and PCL loaded with vancomycin and daptomycin, either added in the form of powder (freestanding) or encapsulated in polymeric microspheres were produced by dip-coating in 316L-SS. Micro-Raman analyses clearly showed the presence of Van and Dap on drug-containing microspheres; however, on multilayered films, the low drug content hindered their detection.

The incorporation of the drug on films was further confirmed during the drug release tests. The release mechanism was proved to be diffusional, and it was demonstrated to be dependent on the pH of media, the type of drug used, and respective encapsulation (microspheres or film).

The daptomycin-loaded films demonstrated antibacterial activity for both MRSA and sensitive *S. aureus* strains, which validates the feasibility of using such films as implant coatings in the mitigation of implant-related *S. aureus* infections.

Overall, this work introduced a new facile processing coating model for protecting metallic implants surface against infections where different antibiotic drugs can be incorporated allowing a long-term release. Further studies to increase control of drug release will be pursued.

■ ASSOCIATED CONTENT

Supporting Information

The Supporting Information is available free of charge at https://pubs.acs.org/doi/10.1021/acsomega.2c00504.

Additional experimental details for substrates surface preparation and peeling-off tests (PDF)

■ AUTHOR INFORMATION

Corresponding Author

Ana Catarina Baptista − *CENIMAT/I3N, Departamento de Ciência dos Materiais, Faculdade de Ciências e Tecnologia, FCT, Universidade Nova de Lisboa, 2829-516 Caparica, Portugal;* orcid.org/0000-0003-1631-6248; Email: anacbaptista@fct.unl.pt

Authors

Íris Soares − *CENIMAT/I3N, Departamento de Ciência dos Materiais, Faculdade de Ciências e Tecnologia, FCT, Universidade Nova de Lisboa, 2829-516 Caparica, Portugal*

Jaime Faria − *CENIMAT/I3N, Departamento de Ciência dos Materiais, Faculdade de Ciências e Tecnologia, FCT, Universidade Nova de Lisboa, 2829-516 Caparica, Portugal*

Ana Marques − *CENIMAT/I3N, Departamento de Ciência dos Materiais, Faculdade de Ciências e Tecnologia, FCT, Universidade Nova de Lisboa, 2829-516 Caparica, Portugal*

Isabel A. C. Ribeiro − *Research Institute for Medicines (iMed.ULisboa), Faculdade de Farmácia, Universidade de Lisboa, 1649-003 Lisboa, Portugal;* orcid.org/0000-0002-7110-6393

Carlos Baleizão − *Centro de Química Estrutural, Institute of Molecular Sciences, Departamento de Engenharia Química, Instituto Superior Técnico, Universidade de Lisboa, 1049-001 Lisboa, Portugal;* orcid.org/0000-0002-7810-1747

Ana Bettencourt − *Research Institute for Medicines (iMed.ULisboa), Faculdade de Farmácia, Universidade de Lisboa, 1649-003 Lisboa, Portugal;* orcid.org/0000-0002-8498-5892

Isabel M. M. Ferreira − *CENIMAT/I3N, Departamento de Ciência dos Materiais, Faculdade de Ciências e Tecnologia, FCT, Universidade Nova de Lisboa, 2829-516 Caparica, Portugal;* orcid.org/0000-0002-8838-0364

Complete contact information is available at: https://pubs.acs.org/10.1021/acsomega.2c00504

Notes

The authors declare no competing financial interest.

■ ACKNOWLEDGMENTS

This work was partially funded by the FEDER funds through the COMPETE 2020 Program and National Funds through the FCT − Portuguese Foundation for Science and Technology under the projects UIDB/50025/2020-2023 (CENIMAT/I3N), PTDC/BTM-SAL/29335/2017, UIDB/04138/2020 and UIDP/04138/2020 (iMed.ULisboa), UIDB/00100/2020 and UIDP/00100/2020 (CQE), and also partially supported by the projects with reference PTDC/CTM-CTM/1571/2020 and ERC-CoG-2014, CapTherPV, 647596. Jaime Faria acknowledges FCT-MEC for the PhD grant with reference PD/BD/143032/2018 grant. The authors would like to thank the use of the traction machine at the Biomaterials Laboratory from the Soft and Bio-functional Materials Group (CENIMAT/I3N).

https://doi.org/10.1021/acsomega.2c00504
ACS Omega 2022, 7, 23096−23106

REFERENCES

(1) Lew, D. P.; Waldvogel, F. A. Osteomyelitis. *Lancet* **2004**, *364*, 369−379.
(2) Arciola, C. R.; Campoccia, D.; Montanaro, L. Implant Infections: Adhesion, Biofilm Formation and Immune Evasion. *Nat. Rev. Microbiol.* **2018**, *16*, 397−409.
(3) Goodman, S. B.; Yao, Z.; Keeney, M.; Yang, F. The Future of Biologic Coatings for Orthopaedic Implants Stuart. *Biomaterials* **2013**, *34*, 3174−3183.
(4) Lamberet, A.; Violas, P.; Buffet-bataillon, S.; Hamel, A.; Launay, E.; Lamberet, R.; Arvieux, C.; Tattevin, P. Postoperative Spinal Implant Infections in Children. *Pediatr. Infect. Dis. J.* **2018**, *37*, 511−513.
(5) Renvert, S.; Polyzois, I. Treatment of Pathologic Peri-Implant Pockets. *Peridontol. 2000* **2018**, *76*, 180−190.
(6) Vasoo, S. Improving the Diagnosis of Orthopedic Implant-Associated Infections: Optimizing the Use of Tools Already in the Box. *J. Clin. Microbiol.* **2018**, *56*, No. e01379-18.
(7) Nandi, S. K.; Mukherjee, P.; Roy, S.; Kundu, B.; De, D. K.; Basu, D. Local Antibiotic Delivery Systems for the Treatment of Osteomyelitis - A Review. *Mater. Sci. Eng. C* **2009**, *29*, 2478−2485.
(8) Mendes, R. M.; Francisco, A. P.; Carvalho, F. A.; Dardouri, M.; Costa, B.; Bettencourt, A. F.; Costa, J.; Gonçalves, L.; Costa, F.; Ribeiro, I. A. C.; Fighting, S. Aureus Catheter-Related Infections with Sophorolipids: Electing an Antiadhesive Strategy or a Release One? *Colloids Surf., B* **2021**, *208*, No. 112057.
(9) Hickok, N. J.; Shapiro, I. M.; Chen, A. F. The Impact of Incorporating Antimicrobials into Implant Surfaces. *J. Dent. Res.* **2018**, *97*, 14−22.
(10) Munasinghe, P. C.; Khanal, S. K. Biomass-Derived Syngas Fermentation into Biofuels. *Biofuels* **2011**, *101*, 79−98.
(11) Roguska, A.; Belcarz, A.; Zalewska, J.; Holdynski, M.; et al. Metal TiO 2 Nanotube Layers for the Treatment of Dental Implant Infections. *Appl. Mater. Interfaces* **2018**, *10*, 17089−17099.
(12) Kiran, A. S. K.; Kumar, T. S. S.; Perumal, G.; Sanghavi, R.; et al. Dual Nanofibrous Bioactive Coating and Antimicrobial Surface Treatment for Infection Resistant Titanium Implants. *Prog. Org. Coat.* **2018**, *121*, 112−119.
(13) Inoue, D.; Kabata, T.; Kajino, Y.; Shirai, T.; Tsuchiya, H. Iodine-Supported Titanium Implants Have Good Antimicrobial Attachment Effects. *J. Orthop. Sci.* **2019**, *24*, 548−551.
(14) Tan, L.; Li, J.; Liu, X.; Cui, Z.; Yang, X.; Zhu, S.; Li, Z.; Yuan, X.; Zheng, Y.; Yeung, K. W. K.; Pan, H.; Wang, X.; Wu, S. Rapid Biofilm Eradication on Bone Implants Using Red Phosphorus and Near-Infrared Light. *Adv. Mater.* **2018**, *30*, No. 1801808.
(15) Guo, S.; Zhu, X.; Loh, X. J. Controlling Cell Adhesion Using Layer-by-Layer Approaches for Biomedical Applications. *Mater. Sci. Eng. C* **2017**, *70*, 1163−1175.
(16) Moseke, C.; Gbureck, U.; Elter, P.; Drechsler, P.; Zoll, A.; Thull, R.; Ewald, A. Hard Implant Coatings with Antimicrobial Properties. *J. Mater. Sci.: Mater. Med.* **2011**, *22*, 2711−2720.
(17) Wan, Y. Z.; Raman, S.; He, F.; Huang, Y. Surface Modification of Medical Metals by Ion Implantation of Silver and Copper. *Vacuum* **2007**, *81*, 1114−1118.
(18) Stewart, S.; Barr, S.; Engiles, J.; Hickok, N. J.; Shapiro, I. M.; Richardson, D. W.; Parvizi, J.; Schaer, T. P. Biofilm Formation and Supports Bone-Healing in an Infected Osteotomy Model in Sheep. *J. Bone Jt. Surg.* **2012**, *94*, 1406−1415.
(19) Kazemzadeh-Narbat, M.; Lai, B. F. L.; Ding, C.; Kizhakkedathu, J. N.; Hancock, R. E. W.; Wang, R. Multilayered Coating on Titanium for Controlled Release of Antimicrobial Peptides for the Prevention of Implant-Associated Infections. *Biomaterials* **2013**, *34*, 5969−5977.
(20) Nablo, B. J.; Rothrock, A. R.; Schoenfisch, M. H. Nitric Oxide-Releasing Sol-Gels as Antibacterial Coatings for Orthopedic Implants. *Biomaterials* **2005**, *26*, 917−924.
(21) Wei, T.; Tang, Z.; Yu, Q.; Chen, H. Smart Antibacterial Surfaces with Switchable Bacteria-Killing and Bacteria-Releasing Capabilities. *Appl. Mater. Interfaces* **2017**, *9*, 37511−37523.
(22) Prodana, M.; Stoian, A. B.; Burnei, C.; Ionita, D. Innovative Coatings of Metallic Alloys Used as Bioactive Surfaces in Implantology: A Review. *Coatings* **2021**, *11*, No. 649.
(23) Shadanbaz, S.; Dias, G. J. Calcium Phosphate Coatings on Magnesium Alloys for Biomedical Applications: A Review. *Acta Biomater.* **2012**, *8*, 20−30.
(24) Kumaravel, V.; Nair, K. M.; Mathew, S.; Bartlett, J.; Kennedy, J. E.; Manning, H. G.; Whelan, B. J.; Leyland, N. S.; Pillai, S. C. Antimicrobial TiO2 Nanocomposite Coatings for Surfaces, Dental and Orthopaedic Implants. *Chem. Eng. J.* **2021**, *416*, No. 129071.
(25) Ishihama, H.; Ishii, K.; Nagai, S.; Kakinuma, H.; Sasaki, A.; Yoshioka, K.; Kuramoto, T.; Shiono, Y.; Funao, H.; Isogai, N.; Tsuji, T.; Okada, Y.; Koyasu, S.; Toyama, Y.; Nakamura, M.; Aizawa, M.; Matsumoto, M. An Antibacterial Coated Polymer Prevents Biofilm Formation and Implant-Associated Infection. *Sci. Rep.* **2021**, *11*, No. 3602.
(26) Tapscott, D. C.; Wottowa, C. Orthopedic Implant Materials. In *StatPearls [Internet]*; StatPearls Publishing: Treasure Island (FL), 2022.
(27) Ferreira, I. S.; Bettencourt, A.; Bétrisey, B.; Gonçalves, L. M. D.; Trampuz, A.; Almeida, A. J. Improvement of the Antibacterial Activity of Daptomycin-Loaded Polymeric Microparticles by Eudragit RL 100: An Assessment by Isothermal Microcalorimetry. *Int. J. Pharm.* **2015**, *485*, 171−182.
(28) Bettencourt, A.; Ferreira, I.; Gonçalves, L.; Kasper, S.; Bertrand, B.; Kikhney, J.; Moter, A.; Trampuz, A.; Almeida, A. J. Activity of daptomycin- and vancomycin-loaded poly-epsilon-caprolactone microparticles against mature staphylococcal biofilms. *Int. J. Nanomed.* **2015**, 4351−4366.
(29) Rezaee, M.; Tsai, L.-C.; Haider, M. I.; Yazdi, A.; Sanatizadeh, E.; Salowitz, N. P. Quantitative Peel Test for Thin Films/Layers Based on a Coupled Parametric and Statistical Study. *Sci. Rep.* **2019**, *9*, No. 19805.
(30) Kokubo, T.; Takadama, H. How Useful Is SBF in Predicting in Vivo Bone Bioactivity? *Biomaterials* **2006**, *27*, 2907−2915.
(31) Martin, V.; Ribeiro, I. A.; Alves, M. M.; Gonçalves, L.; Claudio, R. A.; Grenho, L.; Fernandes, M. H.; Gomes, P.; Santos, C. F.; Bettencourt, A. F. Engineering a Multifunctional 3D-Printed PLA-Collagen-Minocycline-NanoHydroxyapatite Scaffold with Combined Antimicrobial and Osteogenic Effects for Bone Regeneration. *Mater. Sci. Eng. C* **2019**, *101*, 15−26.
(32) Thomas, K. J.; Sheeba, M.; Nampoori, V. P. N.; Vallabhan, C. P. G.; Radhakrishnan, P. Raman spectra of polymethyl methacrylate optical fibres excited by a 532 nm diode pumped solid state laser. *J. Opt. A Pure Appl. Opt.* **2008**, *10*, 055303.
(33) Rygula, A.; Majzner, K.; Marzec, K. M.; Kaczor, A.; Pilarczyk, M.; Baranska, M. Raman Spectroscopy of Proteins: A Review. *J. Raman Spectrosc.* **2013**, *44*, 1061−1076.
(34) Mathematical Models of Drug Release. *Strategies to Modify the Drug Release from Pharmaceutical Systems*; Elsevier, 2015; pp 63−86.
(35) Salina, E. G.; Ekins, S.; Makarov, V. A. A Rapid Method for Estimation of the Efficacy of Potential Antimicrobials in Humans and Animals by Agar Diffusion Assay. *Chem. Biol. Drug Des.* **2019**, *93*, 1021−1025.
(36) Moses, V. K.; Kandi, V.; Rao, S. K. D. Minimum Inhibitory Concentrations of Vancomycin and Daptomycin Against Methicillin-Resistant *Staphylococcus Aureus* Isolated from Various Clinical Specimens: A Study from South India. *Cureus* **2020**, *12*, No. e6749.
(37) Sader, H. S.; Fritsche, T. R.; Jones, R. N. Daptomycin Bactericidal Activity and Correlation between Disk and Broth Microdilution Method Results in Testing of *Staphylococcus Aureus* Strains with Decreased Susceptibility to Vancomycin. *Antimicrob. Agents Chemother.* **2006**, *50*, 2330−2336.
(38) Weinstein, M. P.; Kirn, T. J., II; J, S. L.; Limbago, B.; Bobenchik, A. M.; Mathers, A. J.; Campeau, S.; Mazzulli, T.; Cullen, S. K.; Weinstein, M. P.; Satlin, M.; Galas, M. F.; Schuetz, A. N.; Gold, H.; Patel, J. B.; Humphries, R. M.; Simner, P. J.; Tamma, P. D. *CLSI M100-ED29: 2019 Performance Standards for Antimicrobial Suscepti-*

https://doi.org/10.1021/acsomega.2c00504
ACS Omega 2022, 7, 23096−23106

bility Testing, 29th Edition, 30th ed.; Clinical and Laboratry Standards Institute: Pennsylvanya, 2020.

https://doi.org/10.1021/acsomega.2c00504
ACS Omega 2022, 7, 23096−23106